Distortions in structures of the twist bend nematic phase of a bent-core liquid crystal by the electric field

K. Merkel,[1,*] A. Kocot,[1] J. K. Vij,[2,†] and G. Shanker[3]

[1]*Institute of Material Science, Silesian University, Katowice 40-007, Poland*

[2]*Department of Electronic and Electrical Engineering, School of Engineering, Trinity College Dublin, The University of Dublin, Dublin 2, Ireland*

[3]*Department of Studies in Chemistry, Jnana Bharathi Campus, Sneha Bhavan, Bangalore University, Bangalore 560056, India*

(Received 6 March 2018; published 31 August 2018)

The dielectric spectra of the twist bend nematic phase (N_{TB}) of an achiral asymmetric bent-core liquid crystalline compound are studied for determining the various relaxation modes. Dielectric measurements are also carried out under the bias field E up to 8 V/μm. Two molecular and two collective relaxation processes are observed. The orientational order parameters with respect to the local and the main directors determined using molecular modes are used to find the heliconical angle. The results also show that the order parameter with reference to the main director reverses its trend from increasing to decreasing at temperatures of a few degrees above the N_{TB} to N transition. The collective relaxation modes are assigned to (a) distortions of the local director by the electric field at a frequency of ∼100 kHz while the periodic helical structure remains unaltered (mode attributed to flexoelectricity); (b) changes in the periodic structure arising from a coupling of the dielectric anisotropy with the electric field at the lowest frequency in the range of 100 Hz–10 kHz. Frequency of the higher frequency collective mode (∼100 kHz) depends primarily on the heliconical angle and has anomalous softeninglike behavior at the N-N_{TB} transition. The lowest frequency mode is studied under the bias field E; the modulus of the wave vector gradually vanishes on increasing E (except for an initial behavior, $E^2 < 0.1\,\mathrm{V}^2/\mu\mathrm{m}^2$, which is just the opposite). The transition from the twist bend to splay bend structure is observed by a sudden drop in the frequency of this mode, followed by a linear decrease in frequency by increasing E. The results agree with the predictions made from the currently proposed models for a periodically distorted N_{TB} phase.

DOI: 10.1103/PhysRevE.98.022704

I. INTRODUCTION

Two remarkable physical phenomena for the bent-core liquid crystals were recently revealed. These arise from the polar order and bending of the director. In addition to the four known nematic phases, (i) conventional, (ii) biaxial, (iii) blue, and (iv) cholesteric (chiral nematic), the twist bend nematic (N_{TB}) as the fifth in the sequence of nematic phases has recently been described [1–4]. In this phase the director has uniform bend and twist; the optical axis coincides with the helical one in the absence of external field. The heliconical angle is found to be lower than $\pi/2$ rad. This phase is triggered by the display of anomalously low bent and twist elastic constants of strongly bent shaped molecules. If the polar order exists along the direction orthogonal to the long molecular axis of the bent-core molecules, net polarization emerges which interacts with the electric field. Meyer and Dozov [5] recently showed that the polar order in the transverse direction couples to the bend variations of the main director. The results from an investigation of the response of N_{TB} to the external stimuli such as E or chiral doping [6,7] could lead to a determination of the structure of this phase. An understanding of the phenomenon of the formation of N_{TB} has the potential for practical applications. Nevertheless the structure of this phase and reasons for its formation are not yet fully understood. Physics for the formation of the N_{TB} phase and the effect of external stimuli is a prerequisite for the design of new materials for tailoring to the specific requirements for a given application. The electric field, as the external stimulus, has important advantages, since E is coupled directly to the dielectric anisotropy but is also coupled independently to the polar order. Furthermore, electric field can be conveniently applied across a liquid crystal cell. The phenomenon of flexoelectricity deals with the distortions of the polar order induced by the electric field, whereas ferroelectricity comes into play with the field interacting with the spontaneous polarization. The question as to whether the conventional nematic phase displayed by achiral bent-core systems has ferroelectric properties is being debated [8,9] but this discussion is yet to be extended to the N_{TB} phase.

The physical properties of the material in this phase can be observed through strong dielectric and weak flexoelectric couplings with E [6,7]. The optical axis is rotated by the electric field E, applied in a plane perpendicular to the helical axis [10]. Such a characteristic effect resembles the electroclinic response in SmA^* [11] and the flexoelectric response of a cholesteric nematic (chiral nematic, N^*) [12]. For the case of negative dielectric anisotropy, i.e., when $\Delta\varepsilon < 0$, in the $\boldsymbol{E} \perp \boldsymbol{q}$ geometry of the electroclinic experiment carried out on a planar-aligned cell, the average dielectric torque acting on the helical axis is zero; $\boldsymbol{q}$ is the wave vector. The flexoelectric effect though independent of the dielectric one is operative here. When the high frequency ac probe field is applied, we

*merkelkatarzyna@gmail.com

†jvij@tcd.ie

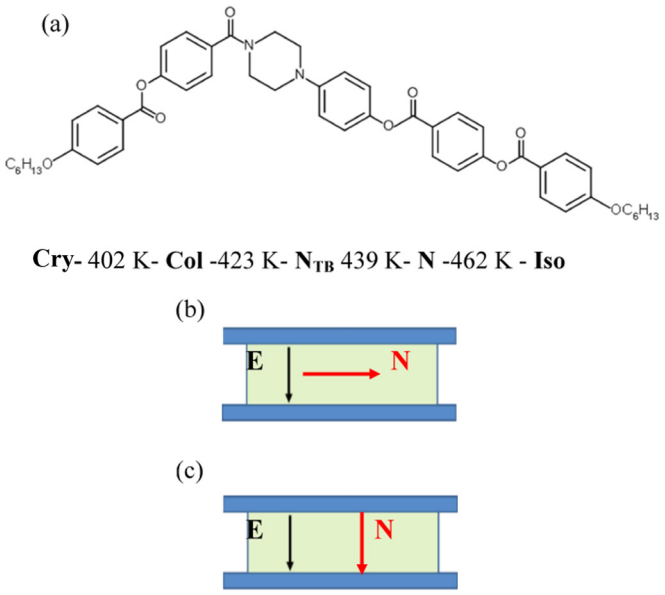

FIG. 1. (a) The chemical structure of an asymmetric bent-core molecule and the phase transition temperatures listed as determined by differential scanning calorimetry (DSC) and polarizing microscopy under cooling from the isotropic state [17]. The schematics of the geometry of sandwich cells for the two alignments are shown as (b) planar, and (c) homeotropic.

can neglect a variation in the wave vector $q(=2\pi/p)$, induced by the probe field, on the assumption that the pitch p of the helical structure is dynamically frozen at its field-off value [13]. At lower frequencies, however, we need to examine the macroscopic effects arising from the bias field. These effects are related to reorganization of the pseudolayers in the N_{TB} phase and with nucleation and propagation of defects in the medium. Our results of dielectric spectroscopy and texture studies under external field are analyzed in terms of models given recently by Matsuyama [14] and Pająk *et al.* [15,16].

II. EXPERIMENT

The chemical structure of an asymmetric bent-core liquid crystal (LC) molecule [17] is given in Fig. 1(a). Wide band dielectric spectroscopic experiments in the frequency range 1 Hz–100 MHz are carried out on a planar-aligned cell with and without the bias field. The cell spacing is varied from 1.6 to 10 μm. Schematics of the geometry of the sandwich cell for both planar and homeotropic alignments are given in Figs. 1(b) and 1(c). The data of dielectric loss ε'' for a planar-aligned LC cell are shown in Figs. 2(a) and 3(a). For the higher frequency dielectric measurements, gold plated cells filled with the material in the isotropic state are used. The alignment layers on the electrodes of the cell are created by coating and annealing the surfactants on the electrodes, prior to the cell's assembly. The amplitude of the probe field lies in the range 0.01–1 V/μm, whereas the dc bias field up to 8 V/μm is applied for studying in detail the lowest frequency mode. Textures of the cell as a function of the external field are recorded and investigated. Textures in the absence of the external field indicate that the planar alignment is successfully obtained. The real (ε') and imaginary (ε'') parts of the complex permittivity are measured for both planar- and homeotropic-aligned cells under slow cooling from the isotropic state. Since the probe field is weak enough, ε' and ε'' correspond to a linear change in the induced polarization brought about by the probe field. In order to determine the dielectric amplitude, $\delta\varepsilon_j$, and the relaxation times, τ_j, of each relaxation mode, the dielectric spectra are analyzed using the Cole-Cole equation (1) that expresses the complex permittivity in terms of the various relaxation processes:

$$\varepsilon^*(\omega) - \varepsilon_\infty = \sum_{j=1}^{n} \frac{\delta\varepsilon_j}{[1 + (i\omega\tau_j)^{1-\alpha_j}]}, \tag{1}$$

Here $\delta\varepsilon_j$, τ_j, α_j, ε_∞ are the fitting parameters of the equation to the experimental data of ε''. We analyzed up to four relaxation peaks ($n \leqslant 4$); however, the low frequency peak is analyzed separately as it does not overlap with other peaks. The corresponding relaxation frequencies, $f_j = 1/2\pi\tau_j$, are calculated from τ_j. A Cole-Cole plot depicts a slightly suppressed arc. The suppression of an arc (the central line of half circle below the ε'' zero value line) is a measure of the nonzero value of the parameter α_j, calculated from the fittings of the experimental data to Eq. (1). From these, α_j is found to be in the range 0.05–0.1. For obtaining a better deconvolution of the relaxation peaks, it is preferable to analyze the derivative

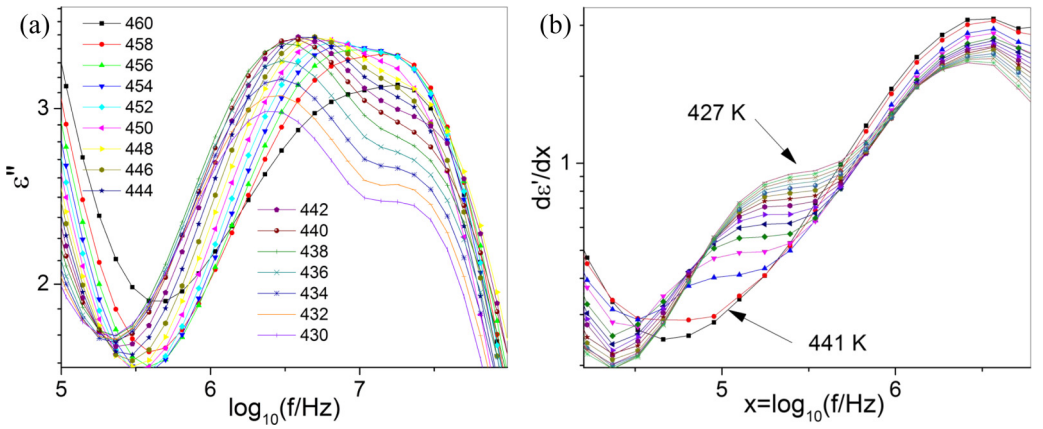

FIG. 2. (a) Dielectric loss ε'' spectra recorded for a planar-aligned cell (thickness = 5 μm) are plotted vs $\log_{10}(f/\mathrm{Hz})$. (b) The derivative, $d\varepsilon'/d\log_{10}(f)$, is plotted vs $\log_{10}(f)$ from its value of 4 - 7. The measuring (probe) field = 0.1 V/μm.

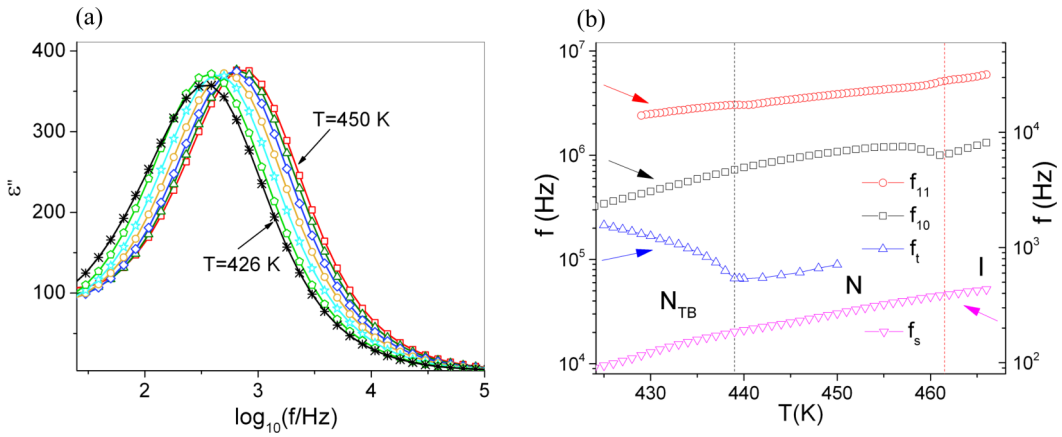

FIG. 3. (a) The ε'' spectra recorded for a planar-aligned cell at low frequencies are plotted at a temperature step of 2 K showing a large polar order. (b) The four relaxation frequencies are plotted vs T. The precessional rotation, f_{10}, (□), and the spinning motion, f_{11}, (○), are assigned to the two molecular modes. The tilt deformation, f_t, (Δ), and f_S, the structural (∇) modes assigned to the collective ones, are plotted as a function of T. The cell spacing $= 5\,\mu$m and the probe field $= 0.1\,\mathrm{V}/\mu$m.

of ε' with respect to $\log_{10}(f)$ [18]; see Fig. 2(b). Relaxation frequencies of the various modes are calculated by fitting the experimental data depicted in Figs. 2(a) 2(b), and 3(a) to Eq. (1). A set of four relaxation frequencies so obtained is plotted vs temperature in Fig. 3(b). The dielectric amplitudes for the two higher frequency modes are plotted in Fig. 4(a).

III. RESULTS AND DISCUSSION

The ε'' spectra reveal two relaxation peaks in the higher frequency range of Fig. 2(a). These are assigned to the molecular relaxation modes. However, the two peaks observed at low frequencies in Figs. 2(b) and 3(a) are assigned to the collective relaxation modes. Different components of the dipole moment contribute to the dielectric permittivity differently and these relax at different frequencies of the probe field. The complex permittivity expressed in terms of the Maier and Meier (M-M) model as given by Toriyama *et al.* [19] is used here. The phenomenon of dielectric relaxation in the nematic phase is usually interpreted in terms of the rotational diffusion model for the reorientation of molecules in the nematic field [20]. The perpendicular component of the dielectric permittivity measured normal to the nematic director in a planar-aligned cell includes contributions for both parallel and perpendicular components of the molecular dipole moment with respect to the long molecular axis.

The perpendicular component of the complex permittivity, $\varepsilon^*_\perp(\omega)$, can be written as [19]

$$\varepsilon^*_\perp(\omega) - \varepsilon_{\perp\infty} \approx \frac{N' h F^2}{3\varepsilon_0 k_B T}\left[\frac{{\mu_t}^2(1-S)}{1+i\omega\tau_{10}} + \frac{{\mu_t}^2\left(1+\frac{1}{2}S\right)}{1+i\omega\tau_{11}}\right]. \quad (2)$$

$A = N' h F^2/3\varepsilon_0 k_B$ is the scaling factor for the two relaxation mechanisms that contribute to the complex permittivity.

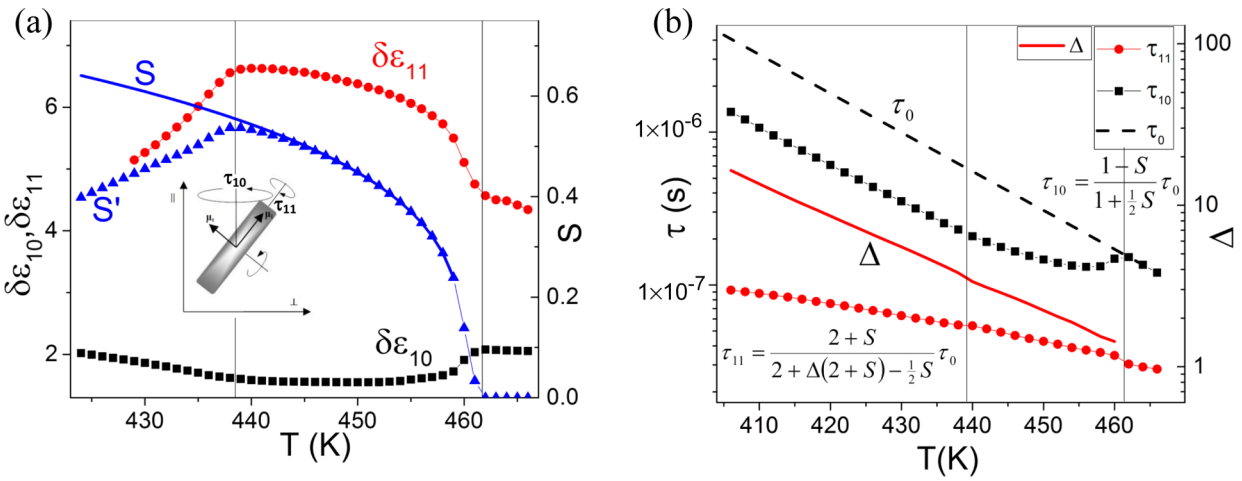

FIG. 4. (a) Plots of the dielectric amplitudes of molecular modes vs temperature: the precessional mode, $\delta\varepsilon_{10}$, (■), and the spinning mode, $\delta\varepsilon_{11}$, (●). The orientational order parameter, S, calculated from τ_{10}/τ_0 is marked as a blue continuous line. The parameter S' is calculated from $\delta\varepsilon_{10}$ and is plotted as, (▲). The inset in Fig. 4(a) shows relaxation mechanisms of τ_{10} and τ_{11}. (b) The two relaxation times, τ_{10}, (■), and τ_{11}, (●), are plotted as a function of temperature. Like the dielectric amplitudes $\delta\varepsilon_{10}$ and $\delta\varepsilon_{11}$, τ_{10} and τ_{11} relate to the precessional and the spinning modes, respectively. τ_0 is the relaxation time in the isotropic phase and is extrapolated to lower temperatures shown by a dashed line in (b). The anisotropy in the rotational diffusion coefficients, Δ, is calculated and plotted as a red continuous line, marked as Δ.

In Eq. (2), $N'(=M/d)$ is the number density of molecules, d is the mass density and M is the molecular weight, ε_0 is the permittivity of vacuum, T is the absolute temperature, and k_B is the Boltzmann constant. F and h are the internal field factors for the reaction and cavity fields, respectively. μ_l and μ_t are the longitudinal and the transverse projections of the molecular dipole moment, μ_0, directed along and normal to the long molecular axis, respectively. Thus depending on the nature of the relaxation mode, the two terms on the right-hand side of Eq. (2) relax at different frequencies, $f_j = 1/2\pi\tau_j$. In the rotational diffusion model [20], τ_{10} and τ_{11} are the relaxation times for the precessional and spinning rotations, respectively, and are so assigned. Expressions for τ_{10} and τ_{11} are related with the relaxation time in the isotropic state, τ_0 by Eqs. (3a) and (3b). The orientational order parameter S and the anisotropy in the rotational diffusion coefficients $\Delta = \frac{1}{2}[D_{||}/D_{\perp} - 1]$ are also expressed by Eqs. 3(a) and 3(b). $D_{||}$ and $D_{\perp}$ are the rotational diffusion coefficients for parallel and normal diffusions to the nematic director, respectively.

$$\frac{\tau_{10}}{\tau_0} = \frac{1-S}{1+\frac{1}{2}S}, \tag{3a}$$

$$\frac{\tau_{11}}{\tau_0} = \frac{2+S}{2+\Delta(2+S)-\frac{1}{2}S}. \tag{3b}$$

In Eqs. (3a) and 3(b), τ_0 is the relaxation time of the LC material in its isotropic phase. $\tau_0 = 3\gamma V/k_B T$, γ is the rotational viscosity, and $V(=d/M = 1/N)$ is the volume per molecule, calculated from the d and M values. Figure 4 (a) shows the temperature dependencies of the dielectric amplitudes $\delta\varepsilon_{10}$, $\delta\varepsilon_{11}$ and the orientational order parameter S. τ_{10} and τ_{11} vs T for the precessional and spinning modes plotted in Fig. 4(b) imply that the rates of relaxation processes in the nematic phase are faster than in the isotropic state, i.e., the relaxation times are lower in the nematic than in the isotropic phase due to the nematic field. The relaxation frequencies, $1/2\pi\tau_{10}$ and $1/2\pi\tau_{11}$, lying in the frequency range 10^6–10^8 Hz correspond to the molecular modes. The scaling factors for τ_{10} and τ_{11} with respect to τ_0 are given in terms of S, and Δ by Eqs. (3a) and (3b). For a conventional nematic phase, however, the results are normally well reproduced by the rotational diffusion model of Coffey and Kalmykov [20]. The order parameter, S, can be calculated either from τ_{10}/τ_0 using Eq. (3a) or from $\delta\varepsilon_{10}$, using the first term in Eq. (2). In order to calculate S from τ_{10}/τ_0, we assume that τ_0 in the isotropic state is described by a thermal activated process (Arrhenius law). S measured with respect to the local director is described by the power law, $(1-\frac{T}{T_{NI}})^{\beta}$; the critical exponent factor $\beta(=0.28)$ is found from the fitting of S to T. Interestingly, no change in S is observed at the N to N_{TB} transition. In order to calculate the order parameter S', with reference to the main director, the first term of Eq. (2) is written as $\delta\varepsilon_{10} = B(1-S')/T$. In the isotropic state $S' = 0$; then $B = A\mu_l^2$, which fixes B. The temperature dependence of S' is plotted in Fig. 4(a), and this coincides with the plot of S in a temperature range of 450–460 K. The temperature dependence of S' distinctly reverses its monotonic trend from increase to decrease with a reduction in temperature, at the transition temperature of 438 K, but this curve also departs from the Maier-Meier model at a temperature of a few degrees above the N_{TB} to N transition temperature [Fig. 4(a)]. As stated before, S' is defined in the sample system of reference (with respect to the main director or $\boldsymbol{q}$ symmetry axis), and is related to S by the equation $S' = P_2(\cos\theta)S$. The experimental value of S' in the N_{TB} phase is reduced from S by the factor $P_2(\cos\theta)$ arising from the tilt of the local director from the helical axis by an angle θ. This calculation is reminiscent of finding the order parameters of SmA to SmC phases with respect to the layer normal. Thus the Legendre polynomial $P_2(\cos\theta)$ is calculated from the ratio S'/S and the cone angle θ is obtained; this approaches 30° for $T = 425$ K. It is clear that θ does not extrapolate to zero at the N_{TB} to N transition but remains finite to a few degrees above the N_{TB}-N transition. The rotational viscosity, γ, for the rotations of the local nematic director is calculated from τ_0.

Δ is calculated from S and τ_{11}/τ_0 using Eq. (3b), and is plotted in Fig. 4(b). We next consider the two low frequency relaxation modes that have been plotted in Figs. 2(b) and 3(a).

For sufficiently large E, the dielectric coupling dominates the free energy density of a twist bend nematic phase. For the high frequency ac signal, the dielectric effect is dominant even for weak fields due to a finite time average of the torque acting on **q** in contrast to the polar effect for which the time average is zero. In most cases, however, the dielectric interaction reorients the macroscopic symmetry axis, $\boldsymbol{N}$, as a result of the sum of the torques that act locally on the director $\boldsymbol{n}$, Fig. 5. A reorganization of the pseudolayered structures of N_{TB} is slow and in order to avoid complications, we assume that E varies rapidly. In such a case, we neglect the variations of $\boldsymbol{q}$ with time by assuming that the helical pitch is dynamically frozen at its field-off value. We consider a specific case when the field stabilizes the macroscopic heliconical structure [13].

Figure 6(a) shows a magnified plot of frequency of the tilt deformation mode, f_t [already shown in Fig. 3(b)] vs temperature. This plot is similar to that of the fluctuations of the director determined from results of the dynamic light scattering experiment [21] carried out on a thermotropic liquid crystalline mixture of a monomer with dimer. The corresponding relaxation time, $\tau_t = 1/2\pi f_t$, in the N_{TB} phase varies from 2 to 0.7 μs for temperatures of 438 to 425 K. This is obtained from a fitting of the dielectric spectra, shown in Fig. 2(b), to the relaxation processes. The relaxation time so calculated is found to be much lower than those calculated from an optical switching experiment (15–11 μs) [17]. The latter results, however, are found for a much higher amplitude of E; such a large field probably reduces the q wave vector. On the contrary, the magnitude of τ_t is found to be rather similar to the optical switching time, $\sim$0.7 μs for the two dimer systems CB7CB and C11CB [4,10,13]. We reproduce the temperature dependence of the high frequency tilt mode centered at $\sim 10^5$ Hz, of the relaxation rate [21] or the response time [13] for the tilt of director $\boldsymbol{n}$:

$$\Gamma_t = 1/\tau_t = 2\pi f_t = \frac{2q^2 K_t \sin^2\theta}{\gamma}, \tag{4}$$

where $K_t = (K_1 + K_2)/2$ is the effective elastic constant for the tilt in the coarse grained director $\boldsymbol{N}$ away from the pseudolayer normal. γ is expected to be continuous at the N-N_{TB} transition temperature. Qualitatively, γ and q^2 have similar temperature dependencies and hence γ/q^2, for simplicity, is assumed to be a constant in Eq. (4); $p = p_0$ for $E = 0$ in the N_{TB} phase and $p_0 \approx 14$ nm [22]. γ is calculated

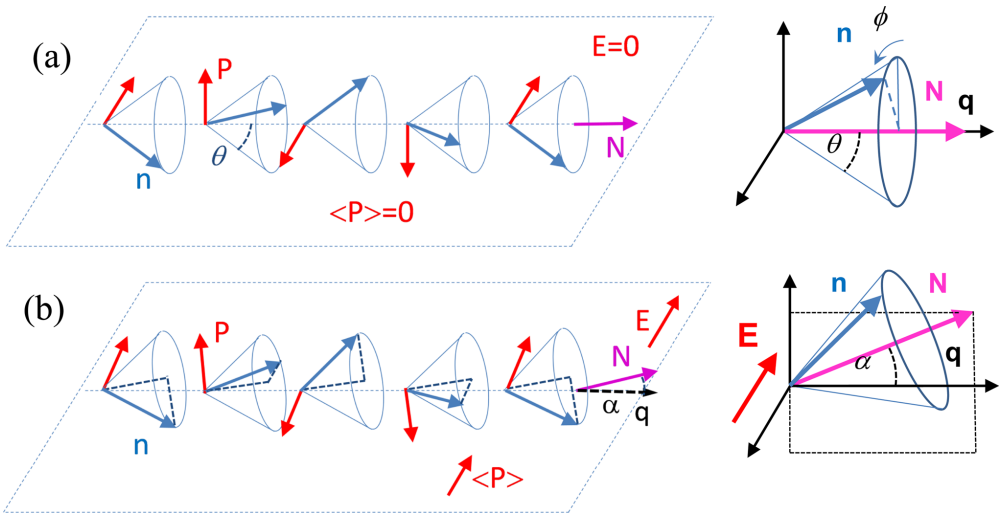

FIG. 5. (a) A demonstration of the electroclinic effect in the N_{TB} phase in the absence of the external field; the local director **n** (blue arrow) follows the heliconical orientation. (b) For the field E applied in a plane normal to the helical axis, the macroscopic optical axis **N** shifts from **q** by an angle α, its magnitude and sign depends on the sign of E and handedness of the twist-bend domain. $\langle \mathbf{P} \rangle$ is the net flexoelectric polarization component directed along E.

from τ_{10} and is found to be 0.9 Pa s at 438 K. The conical angle θ is found to be much greater than $\sim 10^{\circ}$, calculated from the birefringence measurements [17] but the magnitude of this angle is in agreement with that for CB7CB determined from the x-ray scattering experiments [23]. Due to many complexities in the structure of the N_{TB} phase reflected in its texture, the birefringence measurements may be underestimated. Figure 6(a) shows that in N_{TB}, the product, $K_t \sin^2\theta$, obtained from the fitting of Eq. (4) to τ_t, is reproduced by $\sin^2\theta$ alone. This implies that K_t is approximately a constant in the N_{TB} phase. Both curves show similar temperature dependencies; nevertheless a departure observed above the N_{TB}-N temperature is explained by an unusual temperature dependence of K_t, as was observed for some of the elastic constants for CB7CB [24]. It is interesting to note from Fig. 6(a) that θ is already finite for temperatures of a few degrees above the N_{TB}-N transition. The temperature range for which θ is finite coincides with that for the high temperature N_{TB} phase [17], shown in Fig. 6(b).

The lowest frequency (or the longest time) relaxation process is observed in the frequency range 10^2–10^4 Hz. This is identified with the z-dependent rotation of the heliconical director $\mathbf{n}(r)$, which does not change the coarse grained director $\boldsymbol{N}$ [21]. Equivalently, this mode can be regarded as the z-dependent displacement, ϕ/q, of the pseudolayers, leading to alternating compression and dilation of the pseudolayer structure. In the limit of the long wavelength (small q), the relaxation rate is

$$\Gamma_S = 2\pi f_S = \frac{q^2 B_{\mathrm{eff}}}{2\gamma}. \tag{5}$$

B_{eff} is the effective elasticity (associated with K_2 and K_3) [21] which plays the role of the elastic moduli for compression of the pseudolayer structure in the N_{TB} phase. Here γ is the relevant viscosity coefficient. Γ_S is the angular frequency. The relaxation peak of ε'' for the lowest frequency mode plotted in Fig. 3(a) leads to a large dielectric amplitude of $\delta\varepsilon \cong 800$. This

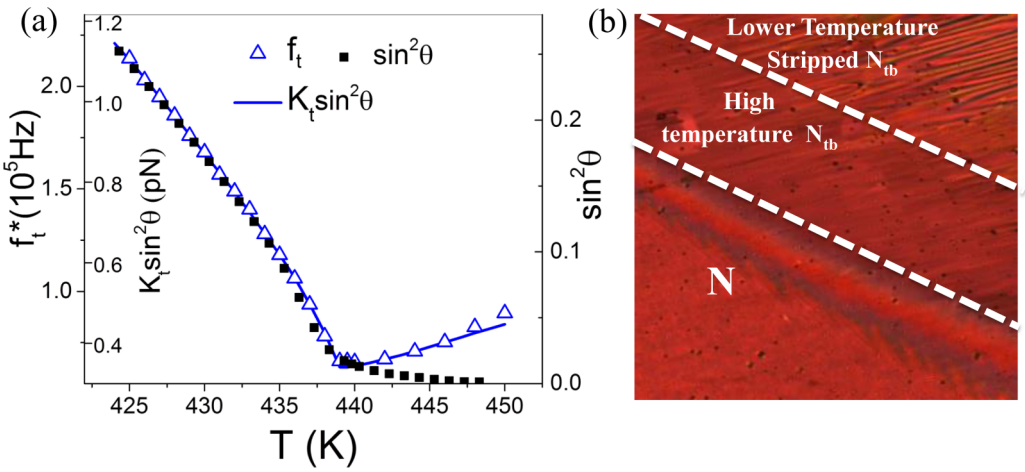

FIG. 6. (a) Relaxation frequency of the helix tilt deformation mode, f_t, (Δ). The continuous blue line is a plot of K_t multiplied by $\sin^2\theta$. Here $K_t \sin^2\theta$ is an unknown parameter obtained from fitting of Eq. (4) to f_t. $\sin^2\theta$ is determined from $\delta\varepsilon_{10}$, (■). $\theta \sim 6^{\circ}$ at the N-N_{TB} transition temperature and rises to 30° at 425 K. (b) Optical polarizing microscopic textures recorded for the N and N_{TB} phases are shown.

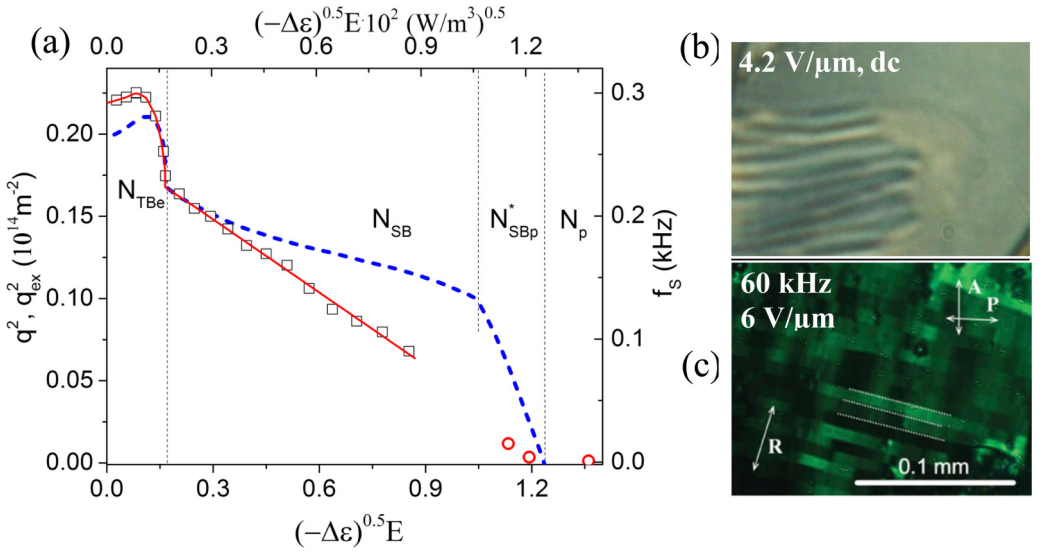

FIG. 7. (a) q^2 plotted as a function of E; this is calculated from the free energy minimization [15] for the ODMNS, shown as a blue dashed line. (For this the X axis is at the bottom and the Y axis is on the left-hand side of the plot.) Peak frequencies and the wave vector for the low frequency mode for $T = 425$ K are plotted. f_S is drawn from the dielectric data (□) and q_{ex}^2, (○), is drawn from texture as a function of the bias field E. (For this the X axis is at the top and the Y axis for f_S is on the right-hand side of the plot.) (b) The textures obtained by application of the dc electric field (4.2 V/μm), and (c) by the sine wave ac electric field (60 kHz, 6 V/μm), are shown.

is obtained from a fitting of the ε'' data to Eq. (1), indicative of a large polar order. The frequency f_S is influenced by the applied electric field E; the field increases the time period and reduces the frequency. It is possible to predict the wave vector, $\boldsymbol{q}$, of the transverse pattern using Eq. (5) for f_S by assuming that the effective elastic constant B_{eff} and the viscosity coefficient γ are field independent. The predicted domain periodicity, found for the elastic constant ($B_{\text{eff}} \approx 10$ pN) lies in the submicron scale (200–900 nm). Such a submicrometer pattern has already been observed using the three-photon excitation fluorescence polarizing microscopy of CB11CB [25,26] and is supported by the observations of templating the polymerization of a mixture of CB7CB with 5 CB in the N_{TB} phase [27]. A theoretical approach for describing the dependence of $\boldsymbol{q}$ on E was given recently by Pająk *et al.* [15], where they calculate the response of the bulk N_{TB} phase to E within the framework of Landau–de Gennes free energy formalism [28]. For a liquid crystalline material with a large negative dielectric anisotropy, $\Delta\varepsilon$, a transformation of the initial phase to the one-dimensional modulated nematic structure (ODMNS) occurs over a wide range of fields. We surmise that E distorts the N_{TB} structure and changes the q value; f_S is found to be proportional to q^2, by Eq. (5). We compare the experimental dependence of q from the dielectric and texture studies with those predicted by the model [15]; comparison is made in Fig. 7(a). Clearly q vanishes on increasing E, whereas the frequency of this mode decreases almost linearly with E. The effect of E is to unwind the structure and to reduce the mode's frequency, except for an initial behavior ($E^2 < 0.1\,\text{V}^2/\mu\text{m}^2$). Such a behavior for low electric field, E, is reminiscent of the Goldstone mode observed in SmC^* phase of ferroelectric liquid crystals (FLCs). The model predicts that the modulation of the main director brought about by negative $\Delta\varepsilon$ interacting with the field undergoes a precession on an elliptic cone around $\boldsymbol{q}$. This leads to an elliptic twist bend phase, N_{TBe}. The stronger fields in the ($\boldsymbol{E}\perp\boldsymbol{q}$) geometry make the base of the elliptic cone narrower and finally the splay bend (N_{SB}) phase is stabilized. The cone is degenerated to a line with the splay bend modulations of $\boldsymbol{n}$. Larger E diminishes the in-plane modulations and the electric polarization P acquires the off-plane uniform component along E. This alternative chiral structure is denoted by N^*_{SBp}. For even larger E this phase transforms to polar nematic, N_{p}, where the polarization is directed parallel to E.

In Fig. 7(a), the experimental data for the N_{TBe} and N_{SB} phases agree qualitatively with the model. The transition from N_{TBe} to N_{SB} is indicated by a sudden drop in the mode's frequency. For N_{SB}, the dependence of q^2 on E falls off more steeply than predicted by the model. It should be noted that the model is valid for the bulk, whereas the real experiments are carried out on a sample confined to a liquid crystal cell. A continuous red line in Fig. 7 guides the experimental data (□). A further increase in E shifts the relaxation peak to frequencies of the ionic processes in the medium. Here q_{ex}^2, determined from the optical textures (○) is plotted vs E. These lie on an extension of the red line for N_{SB}, where the helical structure is gradually unwound by E. This curve represents a linear decrease in the frequency with an increase in the electric field. The texture in Fig. 7(b) shows a transition from the periodic N_{SB} phase to a uniform (unwound) N_{p}. Also the texture under the ac field of 6 V/μm for a frequency of 60 kHz is given in Fig. 7(c). The sharp striped domains indicate that the uniform N^*_{SBp} structure is split into domains that depict left- and right-hand orientations of the director. The birefringence within each domain increases as a function of E, indicative of the N^*_{SBp} structure. The stripe periodicity is found to increase linearly with increase in the time period of the field, similar to that found for achiral dimers with negative dielectric anisotropy [29]. It has, though, not been possible to obtain an unambiguous identification of N^*_{SBp} and N_{p} phases experimentally as predicted by the model.

IV. CONCLUSIONS

An asymmetrical achiral bent-core molecule exhibits both high temperature N and N_{TB} phases over broad ranges of temperature. These observations support the findings that the molecular shape including the angle of bend is the important driving force for the exhibition of N_{TB} phase [30]. The dielectric spectra of the twist bend nematic phase (N_{TB}) of an achiral bent-core liquid crystalline compound are investigated in the frequency range 1 Hz–100 MHz in order to determine its response to the probe field. We observe four modes in the dielectric spectra; the two higher frequency ones are assigned to the molecular modes. These are used to determine the order parameters with respect to the local director as well as with the main director. The two parameters depart from each other at a temperature of a few degrees above the N_{TB} to N transition temperature, indicative of the emergence of a heliconical angle in the high temperature nematic phase followed by an increase of its value with a reduction in temperature in the N_{TB} phase. The two low frequency collective modes are assigned to (a) local distortions of the heliconical angle at a frequency of ∼100 kHz while the periodic helical structure remains unaltered. This mode is attributed to the flexoelectric phenomenon, and (b) changes in the periodic structure arising from a coupling of the dielectric anisotropy to the electric field in the frequency range 100 Hz–10 kHz. The frequency of the higher frequency collective mode given above is shown to depend primarily on the heliconical angle and has anomalous, softeninglike behavior at the N-N_{TB} transition. The lower frequency collective mode is particularly interesting and this corresponds to an alternating compression and dilation of the pseudolayer structure. A large polar order is observed in the N_{TB} phase for the first time. Recent theoretical developments show that the liquid crystalline material with negative dielectric anisotropy when subjected to increasing bias field undergoes a series of transitions from the twist bend to the elliptic twist bend and finally it transits to the splay bend phase. This is corroborated by the experimental results given here by a sudden drop in the frequency of the mode related to the square of the modulus of the wave vector occurring at the N_{TBe} to N_{SB} transition; a further increase in the bias field leads to the polar splay bend phase where the frequency of the mode decreases linearly, whereas the helical pitch increases with an increase in the field. For a large amplitude of the external field, a transition to the polar splay bend phase is observed and finally the helical structure is fully unwound by the field.

ACKNOWLEDGMENTS

We thank Lech Longa (Krakow) and Jonathan Selinger (Kent State) for discussions about recent theoretical developments for the N_{TB} phase. Work of the Dublin group was supported by Science Foundation Ireland (IE), 13/US/I2866 as part of the US–Ireland R and D Partnership program jointly administered with the United States National Science Foundation, NSF-DMR-1410649. The authors (K.M. and A.K.) thank the National Science Centre Poland for Grant No. 2011/03/B/ST3/03369. G.S. acknowledges SERB No. ECR/2016/001224, dt 03.01.207 for the support.

[1] V. P. Panov, M. Nagaraj, J. K. Vij, Yu. P. Panarin, A. Kohlmeier, M. G. Tamba, R. A. Lewis, and G. H. Mehl, Phys. Rev. Lett. **105**, 167801 (2010).
[2] V. Borshch, Y.-K. Kim, J. Xiang, M. Gao, A. Jakli, V. P. Panov, J. K. Vij, C. T. Imrie, M. G. Tamba, G. H. Mehl, and O. D. Lavrentovich, Nat. Commun. **4**, 2635 (2013).
[3] D. Chen, J. H. Porada, J. B. Hooper, A. Klittnick, Y. Shen, M. R. Tuchband, E. Korblova, D. Bedrov, D. M. Walba, M. A. Glaser, J. E. Maclennan, and N. A. Clark, Proc. Natl. Acad. Sci. USA **110**, 15931 (2013).
[4] C. Meyer, G. R. Luckhurst, and I. Dozov, Phys. Rev. Lett. **111**, 067801 (2013).
[5] C. Meyer and I. Dozov, Soft Matter **12**, 574 (2016).
[6] H. J. Deuling, Mol. Cryst. Liq. Cryst. **19**, 123 (1972).
[7] S. M. Shamid, S. Dhakal, and J. V. Selinger, Phys. Rev. E **87**, 052503 (2013); R. Balachandran, V. P. Panov, Y. P. Panarin, J. K. Vij, M. G. Tamba, G. H. Mehl, and J. K. Song, J. Mater. Chem. C **2**, 8179 (2014).
[8] G. Shanker, M. Nagaraj, A. Kocot, J. K. Vij, M. Prehm, and C. Tschierske, Adv. Funct. Mater. **22**, 1671 (2012).
[9] G. Shanker, M. Prehm, M. Nagaraj, J. K. Vij, M. Weyland, A. Eremin, and C. Tschierske, ChemPhysChem **15**, 1323 (2014).
[10] V. P. Panov, R. Balachandran, M. Nagaraj, J. K. Vij, M. G. Tamba, A. Kohlmeier, and G. H. Mehl, Appl. Phys. Lett. **99**, 261903 (2011).
[11] S. Garoff and R. B. Meyer, Phys. Rev. Lett. **38**, 848 (1977).
[12] J. S. Patel and R. B. Meyer, Phys. Rev. Lett. **58**, 1538 (1987).
[13] C. Meyer, Liq. Cryst. **43**, 2144 (2016).
[14] A. Matsuyama, J. Phys. Soc. Jpn. **85**, 114606 (2016).
[15] G. Pająk, L. Longa, and A. Chrzanowska, arXiv:1801.00027v1 [cond-mat. soft].
[16] L. Longa and G. Pająk, Phys. Rev. E **93**, 040701(R) (2016).
[17] S. P. Sreenilayam, V. P. Panov, J. K. Vij, and G. Shanker, Liq. Cryst. **44**, 244 (2017).
[18] R. Balachandran, V. P. Panov, J. K. Vij, G. Shanker, C. Tschierske, K. Merkel, and A. Kocot, Phys. Rev. E **90**, 032506 (2014).
[19] K. Toriyama, S. Sugimori, K. Moriya, D. A. Dunmur, and R. Hanson, J. Phys. Chem. **100**, 307 (1996).
[20] W. T. Coffey and Y. P. Kalmykov, Adv. Chem. Phys. **113**, 487 (2000).
[21] Z. Parsouzi, S. M. Shamid, V. Borshch, P. K. Challa, A. R. Baldwin, M. G. Tamba, C. Welch, G. H. Mehl, J. T. Gleeson, A. Jakli, O. D. Lavrentovich, D. W. Allender, J. V. Selinger, and S. Sprunt, Phys. Rev. X **6**, 021041 (2016).
[22] D. Chen, M. Nakata, R. Shao, M. R. Tuchband, M. Shuai, U. Baumeister, W. Weissflog, D. M. Walba, M. A. Glaser, J. E. Maclennan, and N. A. Clark, Phys. Rev. E **89**, 022506 (2014).
[23] D. M. Agra-Kooijman, G. Singh, M. R. Fisch, M. R. Vengatesan, J.-K. Song, and S. Kumar, Liq. Cryst. **44**, 191 (2017).
[24] C. J. Yun, M. R. Vengatesan, J. K. Vij, and J.-K. Song, Appl. Phys. Lett. **106**, 173102 (2015); R. Balachandran, V. P. Panov, J. K. Vij, A. Kocot, M. G. Tamba, A. Kohlmeier, and G. H. Mehl, Liq. Cryst. **40**, 681 (2013).
[25] V. P. Panov, J. K. Vij, and G. H. Mehl, Liq. Cryst. **44**, 147 (2017).

[26] V. P. Panov, J. K. Vij, R. Balachandran, V. Borsch, O. D. Lavrentovich, M. G. Tamba, and G. H. Mehl, Proc. SPIE **8828**, 88280X (2013); V. P. Panov, M. C. M. Varney, I. I. Smalyukh, J. K. Vij, M. G. Tamba, and G. H. Mehl, Mol. Cryst. Liq. Cryst. **611**, 180 (2015).

[27] V. P. Panov, S. P. Sreenilayam, Y. P. Panarin, J. K. Vij, C. Walsh, and G. H. Mehl, Nano Lett. **17**, 7515 (2017).

[28] P. G. de Gennes and J. Prost, *The Physics of Liquid Crystals*, 2nd ed. (Clarendon Press, Oxford, 1993).

[29] V. P. Panov, R. Balachandran, J. K. Vij, M. G. Tamba, A. Kohlmeier, and G. H. Mehl, Appl. Phys. Lett. **101**, 234106 (2012).

[30] E. E. Pocock, R. J. Mandle, and J. W. Goodby, Soft Matter **14**, 2508 (2018).